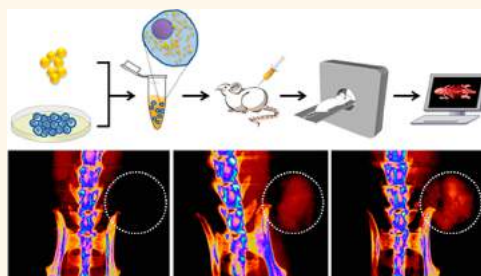


Nanomedicine for Cancer Immunotherapy: Tracking Cancer-Specific T-Cells *in Vivo* with Gold Nanoparticles and CT Imaging

Rinat Meir,^{†,‡} Katerina Shamalov,^{†,‡} Oshra Betzer,[†] Menachem Motiei,[†] Miryam Horovitz-Fried,[‡] Ronen Yehuda,[§] Aron Popovtzer,^{||} Rachela Popovtzer,^{*,†} and Cyrille J. Cohen^{*,‡}

[†]Faculty of Engineering and the Institute of Nanotechnology and Advanced Materials, Bar-Ilan University, Ramat Gan 52900, Israel, [‡]Laboratory of Tumor Immunology and Immunotherapy, Goodman Faculty of Life Sciences, Bar-Ilan University, Ramat Gan 52900, Israel, [§]The Mina and Everard Goodman Faculty of Life Sciences, Bar-Ilan University, Ramat-Gan 52900, Israel, and ^{||}Davidoff Cancer Center, Rabin Medical Center, Beilinson Campus, Petah Tiqwa 49100, Israel. [‡]These authors contributed equally to this work.

ABSTRACT Application of immune cell-based therapy in routine clinical practice is challenging due to the poorly understood mechanisms underlying success or failure of treatment. Development of accurate and quantitative imaging techniques for non-invasive cell tracking can provide essential knowledge for elucidating these mechanisms. We designed a novel method for longitudinal and quantitative *in vivo* cell tracking, based on the superior visualization abilities of classical X-ray computed tomography (CT), combined with state-of-the-art nanotechnology. Herein, T-cells were transduced to express a melanoma-specific T-cell receptor and then labeled with gold nanoparticles (GNPs) as a CT contrast agent. The GNP-labeled T-cells were injected intravenously to mice bearing human melanoma xenografts, and whole-body CT imaging allowed examination of the distribution, migration, and kinetics of T-cells. Using CT, we found that transduced T-cells accumulated at the tumor site, as opposed to nontransduced cells. Labeling with gold nanoparticles did not affect T-cell function, as demonstrated both *in vitro*, by cytokine release and proliferation assays, and *in vivo*, as tumor regression was observed. Moreover, to validate the accuracy and reliability of the proposed cell tracking technique, T-cells were labeled both with green fluorescent protein for fluorescence imaging, and with GNPs for CT imaging. A remarkable correlation in signal intensity at the tumor site was observed between the two imaging modalities, at all time points examined, providing evidence for the accuracy of our CT cell tracking abilities. This new method for cell tracking with CT offers a valuable tool for research, and more importantly for clinical applications, to study the fate of immune cells in cancer immunotherapy.



KEYWORDS: cell tracking · cell therapy · computed tomography · T cells · cancer · imaging · immunotherapy

The idea of cell-based therapy has existed for decades, with recent advances in technology allowing research in the field to progress from preclinical to advanced clinical trials.¹ However, as exciting as it may seem, applying cell-based therapy in routine clinical practice has proven to be very challenging.² Clinical trials have begun to test cell transplantation in human patients, but the results of these trials have been highly mixed; while some patients exhibit major improvement, others experience modest (if any) clinical benefit. This variability in therapeutic outcome exists not only between different trials and centers but also within groups of patients

treated at the same center.³ It remains unclear whether the different outcomes are driven by individual diversity in inherent physiological reactions or rather by factors related to the cell transplantation procedure itself, such as suboptimal injection, poor cell survival, or variations in cell differentiation, biodistribution, and final fate.⁴ At present, the only means for assessing response to cell-based treatment is evaluation of disease symptoms, which often are not quantitative and can only be examined weeks after treatment. Important issues remain unclear, including optimal cell dosage and route of delivery, biology, and safety of transplanted cells, viability, migration, and

* Address correspondence to cyrille.cohen@biu.ac.il (C.J.C., cancer immunotherapy), rachela.popovtzer@biu.ac.il (R.P., cell tracking).

Received for review March 31, 2015 and accepted June 3, 2015.

Published online June 03, 2015
10.1021/acsnano.5b01939

© 2015 American Chemical Society

engraftment of the cells, and their interaction with the microenvironment. These issues prevent the cell therapy field from reaching its full potential. It is therefore critical to develop a reliable, noninvasive, real-time means to image and trace small groups of cells within large tissue volumes and continuously evaluate their biodistribution, final fate, and functionality post-transplantation.

Currently, the most common, and mainly preclinical, method for cell tracking is optical-based fluorescence (or bioluminescent) imaging, in which genetically engineered reporter genes are used for labeling cells.^{5,6} The main advantages of this method are that reporter genes are expressed as long as the cells are vital and are not diluted even after cell division.⁵ However, optical imaging has several crucial limitations, including low tissue penetration of light, which prevents imaging of deep body structures, a projection technique that is only two-dimensional, and no quantification capabilities.⁷ These crucial limitations, in addition to the method's inability to be applied clinically, are quite restraining.

Computed tomography (CT) is one of the leading radiology technologies applied in the field of biomedical imaging.⁸ CT is characterized by high temporal and spatial resolution, and it is among the most convenient imaging tools used in hospitals to date in terms of availability, efficiency, and cost. CT provides superior visualization of bone structures due to the inherent contrast between electron-dense bones and the more permeable surrounding soft tissues. Thus, it is a leading candidate modality for cell tracking and imaging. However, CT is limited in distinguishing between different soft tissues that have similar densities and therefore cannot be used on its own for cell imaging.⁹ A new promising candidate for cell labeling and imaging is nanoparticles, which enable deep body tissue imaging using various modalities.^{10–15} Nanoparticles can be synthesized from various metals, including gold, an element highly suitable for medical applications due to its inert and nontoxic nature as well as its unique physical, chemical, and optical properties. Moreover, gold nanoparticles (GNPs) are easy to synthesize, and their size and shape can be precisely controlled. GNPs are optimal contrast agents for CT imaging due to their high atomic number and electron density,^{16–21} which enhance delineation of soft tissue structures with similar or identical contrast properties.

T-cell based immunotherapy has recently emerged as a promising treatment for advanced cancer.²² Immunotherapeutic drugs recently approved by the FDA, such as immune checkpoint inhibitors (anti-CTLA-4 and anti-PD1 agents), have demonstrated a role for cellular immunity in general, and T-cells in particular, in performing immune surveillance functions.^{23,24} Moreover, direct use of tumor-specific cytotoxic T-cells for cancer treatment has increased over the past 20 years,

and studies have shown that these cells mediate complete tumor regression in metastatic cancer patients.^{25–27} T-cells can be either isolated and expanded from resected tumors (tumor infiltrating lymphocytes) or genetically engineered to express a tumor-specific receptor.²⁸ The latter can be derived from an antibody (chimeric antigen receptor, CAR) or from a T-cell receptor (TCR).^{29,30} An initial description of successful TCR gene therapy for melanoma patients was reported by Morgan et al., using T-cells transduced to express a MART-1 specific TCR termed F4.³¹ We further showed that such an approach may be enhanced at the protein level (TCR structure)^{32–35} or by improving cellular function.^{36,37}

However, further advancement of T-cell based therapy requires methods that can overcome the challenges of clinical treatment. We propose a novel, clinically applicable methodology for noninvasive longitudinal and quantitative tumor-specific T-cell tracking based on the combination of CT as an imaging modality and gold nanoparticles (GNPs) as labeling agents.³⁸ Herein, primary human T-cells that were transduced to express melanoma-specific TCR (targeted T-cells), or nontransduced primary human T-cells (nontargeted T-cells) were uploaded with GNPs. *In vitro* cytokine release and proliferation assays revealed that GNP labeling did not hamper T-cell function. Labeled cells were adoptively transferred to melanoma-bearing mice, and whole-body *in vivo* CT imaging enabled examination of the distribution, migration, and persistence of T-cells in the tumor vicinity (Figure 1). GNP-labeled targeted T-cells were also functional *in vivo*, as they mediated significant tumor regression. The present study also addressed one of the main challenges associated with development of a nanoparticle-based cell tracking approach, namely verifying that the injected T-cells are those that are actually tracked rather than GNPs excreted from the cells. To this end, T-cells were genetically engineered to express green fluorescent protein (GFP) prior to GNP loading, and CT and fluorescence imaging were compared after injection. This proof-of-principle study showed a direct correlation between fluorescence imaging and CT imaging.

RESULTS AND DISCUSSION

To allow sensitive imaging, the T-cells must first be labeled *in vitro* with GNPs as contrast agents (Figure 1); yet it is crucial that the particles have a minimal effect on cell function. Therefore, we performed a comprehensive *in vitro* study on T-cell function, viability, and proliferation following GNP labeling.

GNP Synthesis and Characterization. On the basis of a well-established procedure,^{38–40} 20 nm GNPs were synthesized and then coated with glucose due to its stability and high cell-uptake rate. The particles were characterized using transmission electron microscopy (TEM) and UV–vis spectroscopy (Figure 2).

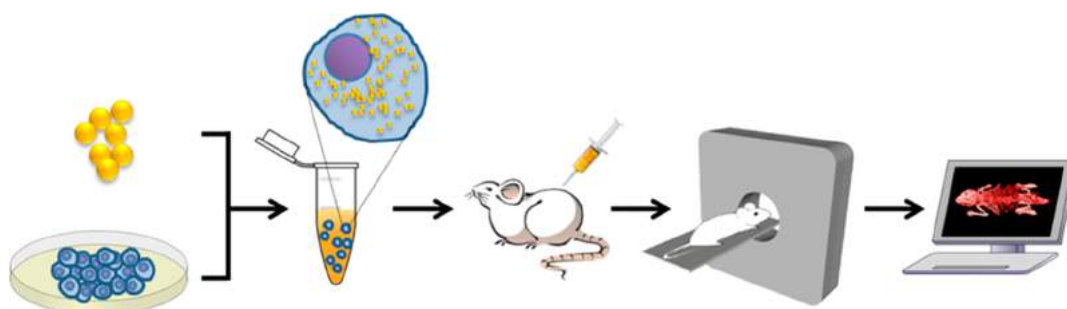


Figure 1. T-cell tracking process. T-cells were labeled with GNPs *in vitro*; the cells were then injected into mice and tracked *in vivo* using CT imaging.

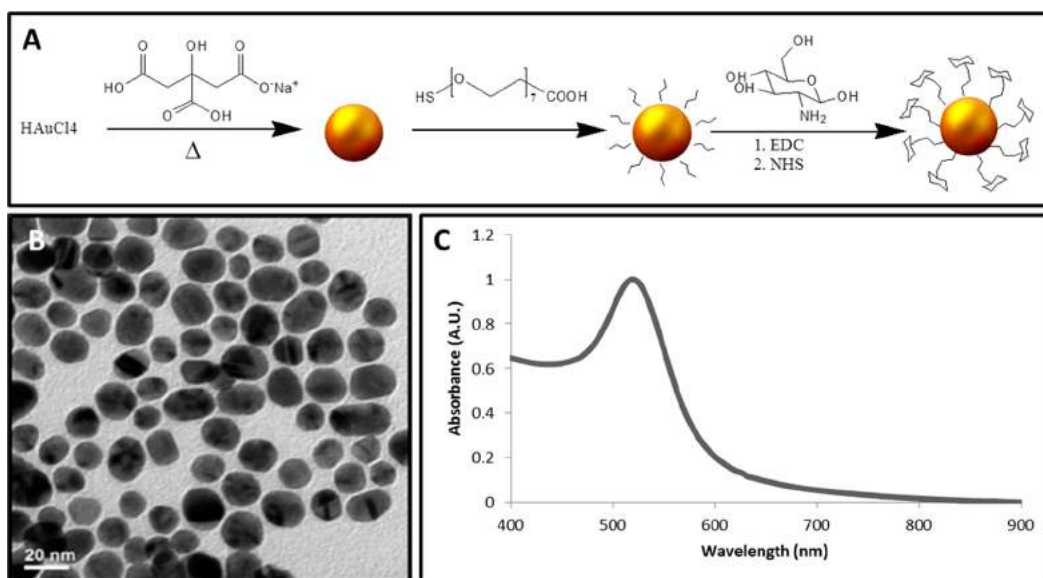


Figure 2. GNP synthesis and characterization. (A) Schematic diagram of the GNP synthesis process: GNPs were conjugated to the linker polyethylene glycol (PEG), followed by covalent conjugation to glucose. (B) Transmission electron microscopy image of 20 nm GNPs. (C) Optical properties of the GNPs as assessed by ultraviolet–visible spectroscopy.

***In Vitro* Labeling of T-Cells with GNPs.** Primary human T-cells were transduced to express a melanoma-specific TCR. We used the F4 TCR,⁴¹ which is specific for HLA-A2/MART-1 antigen^{27–35} and was shown to mediate tumor regression in patients with metastatic melanoma.³¹ The transduced T-cells were then labeled with GNPs at different concentrations (0.38, 0.57, 0.75, and 1 mg/mL) and incubated for different time intervals (20, 60, and 120 min).

To test their biological activity, GNP-loaded primary human T-cells were cocultured with either HLA-A2+/MART-1+ 888-A2, SK-MEL-23, or 888 (HLA-A2-/MART-1+, negative control) human melanoma cell lines for 18 h. T-cell function assessed by IFN γ secretion in cells pre- or postloaded with GNPs at different time points revealed a moderate reduction in cytokine secretion as a function of time (15.2% less IFN secretion for 60 min loading time, and 21.8% less IFN secretion for the 120 min loading time, as compared with the 20 min loading time of T-cells cocultured with 888-A2; Figure 3). Furthermore, comparison of multiple gold loading concentrations showed that cell function was

impaired mostly for the higher gold concentrations (0.75 and 1 mg/mL) after 120 min of incubation (21% and 25% less IFN secretion in coculture with 888-A2 cells, respectively, compared to preloaded T-cells Figure 3C,D). No significant cytokine secretion was noted in cocultures with control 888 melanoma line or preloaded–loaded T-cells for any of the incubation time points or gold concentrations (Figure 3A–C).

We next assessed the proliferation of GNP-loaded F4-expressing T-cells by CFSE labeling followed by stimulation with plate-bound OKT3. Three days after stimulation, the cells were analyzed for CFSE dilution. As seen in Figure 4A, no significant difference in the proliferative capacity of cells loaded with different concentrations of gold was observed at the different time points. However, beyond 20 min loading time, a time-dependent reduction occurred in cell proliferation ability (19.1% reduction in proliferation for 60 min loading time and 34.8% reduction for 120 min loading time, compared to the proliferation observed for 20 min loading time).

We additionally evaluated the effect of GNPs on T-cell viability. Propidium iodide (PI) was added to the

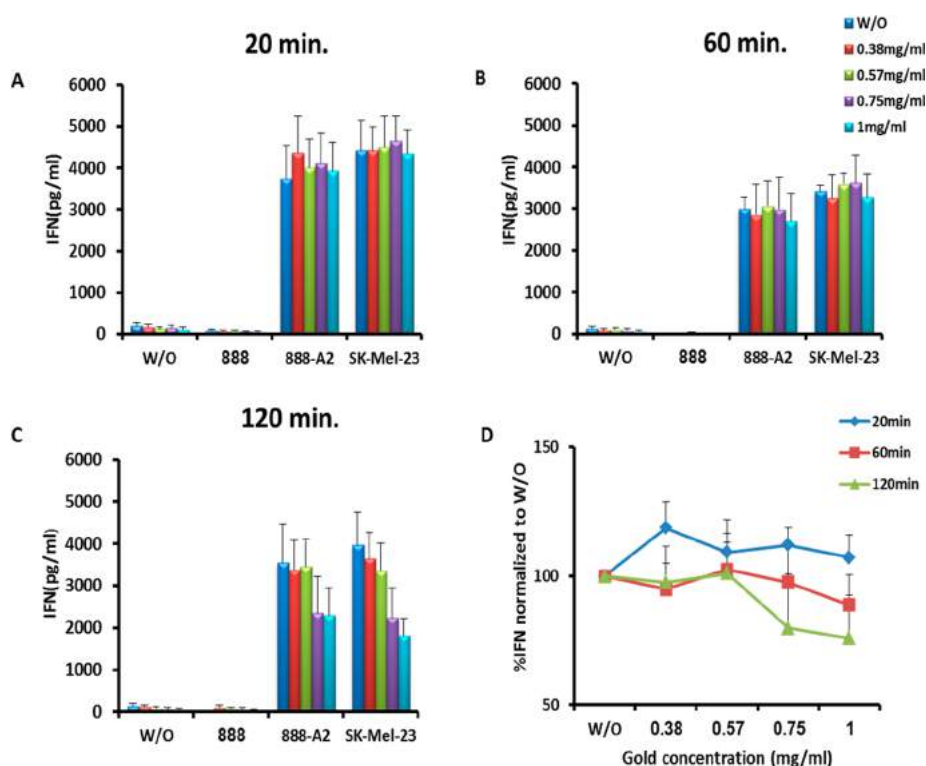


Figure 3. Function of GNP-loaded F4-transduced human T-cells. TCR-transduced primary human T-cells were loaded with different concentrations of gold (0.38, 0.57, 0.75, and 1 mg/mL) and cocultured with multiple melanoma lines, as indicated. IFN- γ secreted in the coculture supernatant was measured by ELISA. Data shown as average secretion from three different donors. Secretion data for each time point (20, 60, and 120 min) is displayed separately (A, B, and C, respectively). (D) IFN secretion of F4-T-cells after coculture with positive target tumor cell line (888-A2) was normalized to control (cells without (w/o) GNPs; $p < 0.05$, Student's paired t test). Results presented as mean \pm SEM ($n = 3$).

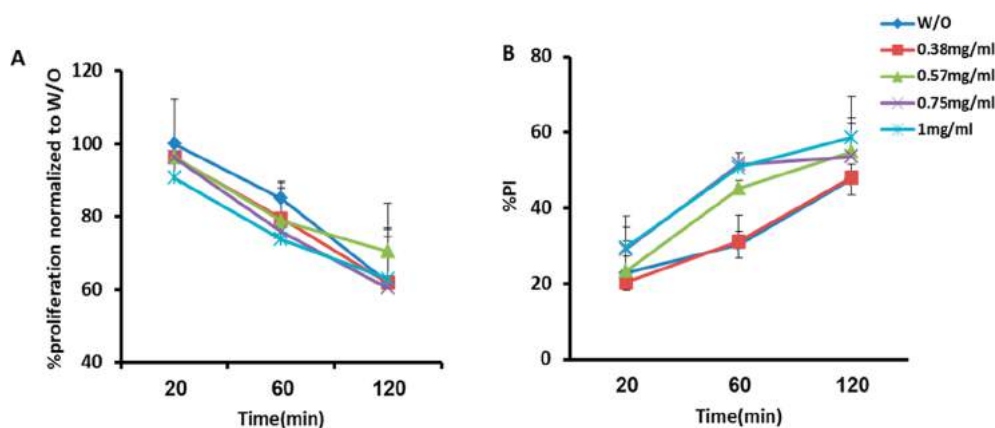


Figure 4. Proliferation and viability of GNP-loaded F4-expressing T-cells. (A) Proliferation assay: CFSE-labeled T-cells loaded with different amounts of gold were stimulated with plate-bound stimulating antibody OKT3 (0.1 mg/mL) in the presence of 30 IU/mL IL-2 (day 0). Three days after stimulation, cells were analyzed for CFSE dilution. Data shown as mean percentage of proliferative cells from three different donors, normalized to control (cells without (w/o) GNPs). Cell proliferation values were measured by dividing the mean fluorescence intensity (MFI) values of day 0 by the MFI of day 3. (B) Viability assay: F4-expressing T-cells were loaded with different GNP concentrations (0.38, 0.57, 0.75, and 1 mg/mL) and cultured for 20, 60, or 120 min. PI was added to the supernatant, and the cells were analyzed by flow cytometry. Data shown as mean percentage of positive PI cells from three different donors. Results presented as mean \pm SEM ($n = 3$).

gold-loaded cells, and PI positivity was assessed by flow cytometry. While there was no significant difference in cell viability for the different gold concentrations at 20 min loading time, increased incubation intervals resulted in a higher loss of viability, especially as the concentration of gold increased (1.5-fold more

cell death for 60 min and more than 2-fold for 120 min, compared to the proportion of cell death for 20 min incubation; Figure 4B).

T-cell loading efficiency was evaluated by the amount of GNP uptake as a function of incubation time (20, 60, or 120 min) and GNP concentration

(0.75 or 1 mg/mL), using flame atomic absorption spectroscopy (FAAS). As seen in Figure 5, gold uptake was similar for the different loading times and concentrations.

On the basis of these results, we established a labeling protocol for T-cells in which 60 min incubation with 0.75 mg/mL GNPs allow for efficient labeling while maintaining optimal biological activity of the T-cells. Using this protocol, we assessed GNP-labeled T-cells with dark-field microscopy. As demonstrated in Figure 6, there is a large accumulation of GNPs within the T-cells after incubation of 60 min.

In Vivo T-Cell Tracking. For the *in vivo* experiments, we compared between T-cells transduced to express a melanoma-specific TCR (targeted T-cells) and non-transduced T-cells (nontargeted T-cells) as control. The two groups of cells were genetically engineered to express GFP, a reporter gene enabling visualization of live cells⁴² with fluorescence imaging (FLI), and then

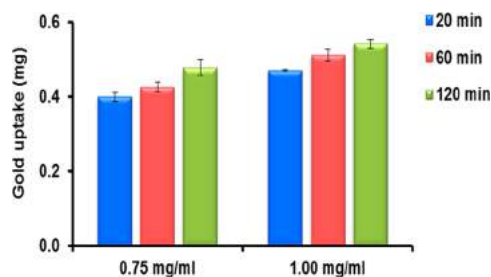


Figure 5. Amount of gold uptake by T-cells measured using FAAS analysis. T-cells were incubated with GNPs (0.75 or 1 mg/mL) for 20, 60, and 120 min. Gold uptake was then determined using FAAS; the concentration in each sample was measured according to its absorbance value, correlated to a calibration curve. Results presented as mean \pm SEM ($n = 3$).

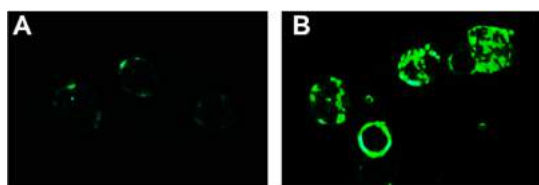


Figure 6. Dark field image intensity of T-cells loaded with GNPs (A) before incubation with GNPs and (B) 60 min after incubation with GNPs.

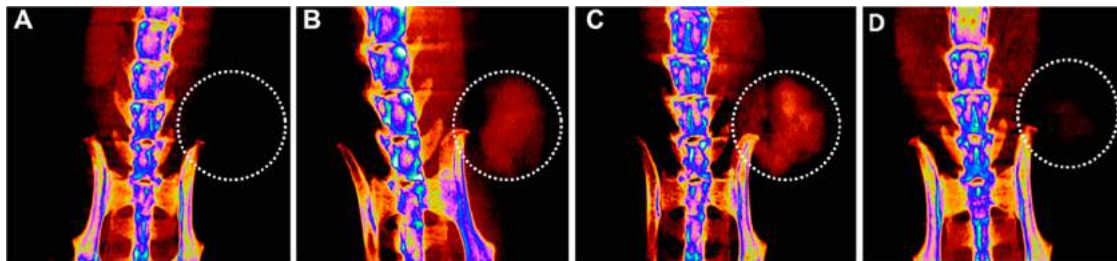


Figure 7. Time-dependent accumulation of targeted T-cells at the tumor. Maximum intensity projection of micro-CT scans (A) before T-cell injection, (B) 24 h post injection, (C) 48 h post injection, and (D) 72 h post injection. Circles demarcate the T-cell accumulation.

loaded with GNPs, using the labeling protocol established above, for CT imaging. These dual-labeled T-cells were injected intravenously into tumor-bearing immune-deficient mice. First, we examined our GNP-based CT imaging technique for longitudinal cell tracking and imaging at several time points. Next, to evaluate the reliability of our method, the CT scans were compared to whole-body FLI.

In Vivo Tracking of the “Golden” T-Cells Using CT. CT imaging has several important advantages for clinical applications, namely providing superior visualization and analysis capabilities so that results can be presented in different perspectives, such as maximum intensity projection, and two-dimensional (2D) or three-dimensional (3D) volume rendering images. Herein, we employed these different imaging perspectives to compare the migration of targeted and nontargeted T-cells. Images were obtained before injection and up to 5 days after injection by using a micro-CT device. The projection images were reconstructed into cross-sectional slices.

Figure 7 shows maximum intensity projection at the tumor site and demonstrates migration of the GNP-labeled targeted T-cells to the tumor area. Before injection, this small tumor cannot be observed using CT scans (Figure 7A). Then 24 h after injection of the GNP-labeled targeted T-cells, a clear CT signal can be observed at the tumor site (Figure 7B) due to the concentration of GNPs within the T-cells that migrate to the tumor site. After 48 h, the signal intensified, indicating an increase in the amount of targeted T-cells at the tumor site (Figure 7C). After this time point, the signal decreased (Figure 7D), and 5 days later, no signal was observed in the tumor area (see Supporting Information, Figure S11). It is possible that after this time period T-cells which were subjected to repetitive encounters with tumor cells could undergo antigen-induced cell death (AICD) or death by apoptosis following the activation of the Fas pathway.⁴³ Additionally, it is possible that human T-cells engraftment in nude mice recipient might be reduced over the course of a few days due to their susceptibility to cytotoxicity by resident murine NK cell populations or the lack of compatible positive costimulatory or cytokine signals lacking in mouse hosts.⁴⁴ Remarkably, in the nontargeted

T-cell group, no signal increase was observed at any time point (see Supporting Information, Figure S12). These images provide, for the first time, evidence for the migration of targeted T-cells to tumor site using CT imaging.

On the basis of our previous study³⁸ in which we established a CT quantitative ruler that can extrapolate

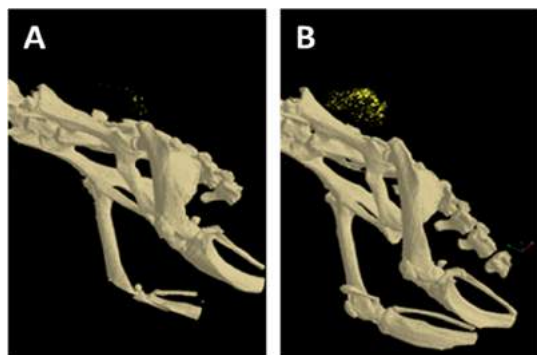


Figure 8. 3D volume-rendering images of T-cell accumulation in the tumor, over time: (A) 4 h post injection, minor accumulation of T-cells can be observed; (B) 48 h post injection, substantial accumulation of T-cells can be seen (yellow).

the cell number in each region of interest in a non-destructive manner, we estimate that 260000 T-cells (1.3% of ID) reached the tumor after 24 h, 460000 after 48 h (2.3% of ID), and 80000 after 72 h (0.4% of ID).

We additionally examined migration and accumulation of the targeted T-cells at the tumor area, over time, using 3D whole-body volume rendering CT imaging. Figure 8 demonstrates that while only minimal accumulation of T-cells could be observed 4 h after injection, considerable accumulation occurred 48 h later.

We further evaluated whole-body biodistribution and migration of the targeted GNP-labeled T-cells, using 2D and 3D volume rendering *in vivo* CT imaging. Then 48 h after injection, the labeled cells can be clearly seen in the lungs (Figure 9A,B,D) and spleen (Figure 9A,C), indicating significant amounts of T-cells that migrated to these organs.

Two weeks post injection, an *ex vivo* analysis using flame atomic absorption spectroscopy was conducted, revealing that insignificant amounts of gold remained in the different organs. Thus, it is clear that the GNPs were secreted out of the body.

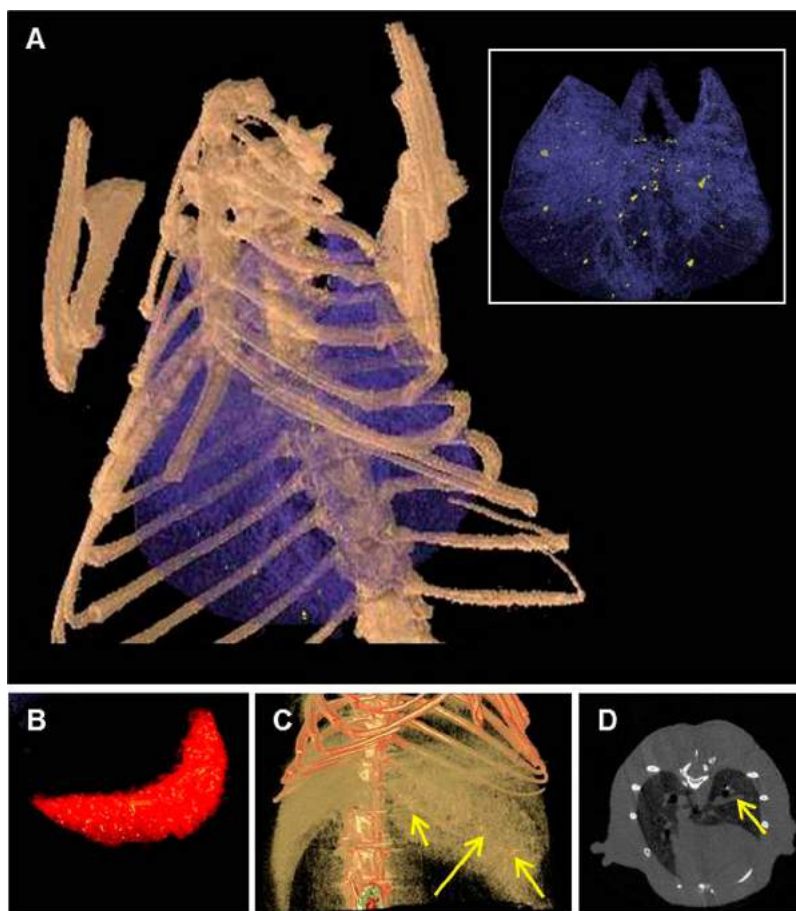


Figure 9. CT scan of whole-body biodistribution and migration of the “golden” T-cells: (A) 3D volume rendering CT image of T-cells that accumulated in the lungs 48 h post injection (inset: 3D image of lungs; yellow areas are GNP-labeled T-cells); (B) 3D image of spleen; (C) 3D image of liver; (D) representative 2D CT image of lungs, arrow indicating gold-labeled cells.

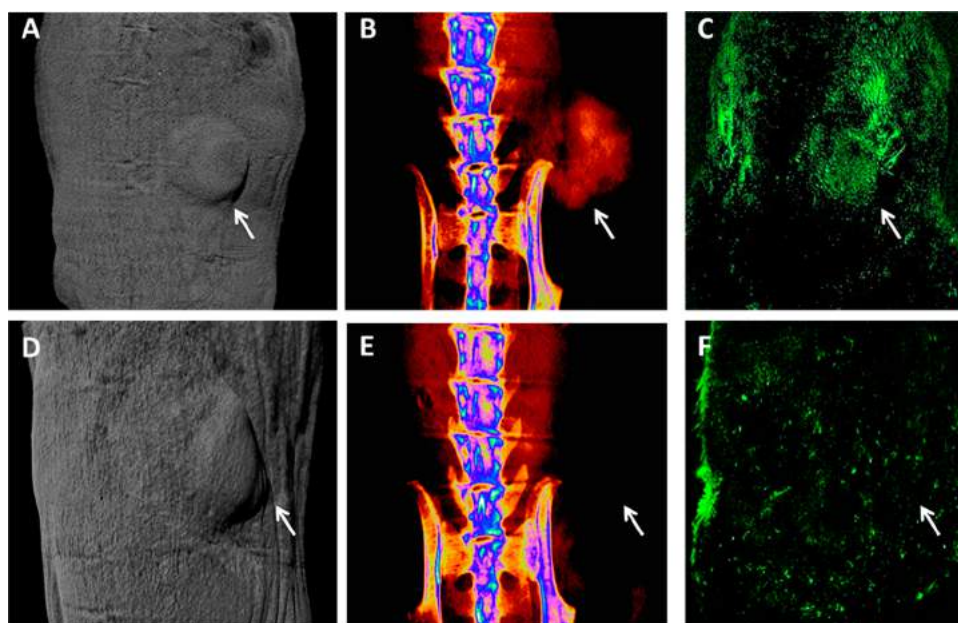


Figure 10. Comparison of CT to FLI for targeted T-cells (A–C) and nontargeted T-cells (D–F). (A,D) 3D CT images indicating location of tumor. (B,E) MPI CT images of the tumor area. (C,F) GFP fluorescence imaging. The images demonstrate a direct correlation between FLI and CT imaging of the tracked T-cells. The presented images were obtained 48 h post injection at maximal accumulation of the targeted-T-cells at the tumor site.

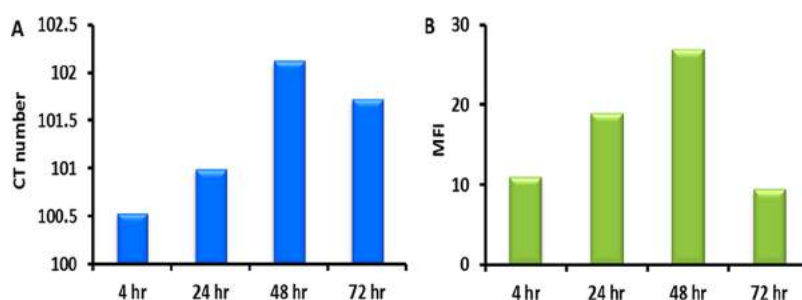


Figure 11. Quantitative comparison of CT and fluorescence signals over time in a single mouse. (A) Average CT numbers of the tumor area. CT number was measured as arbitrary units by gray values of gold enhancement. (B) Maximum fluorescence intensity (MFI) measured at the tumor area. Measurements were calculated as average intensity over the tumor surface area by using ImageJ software. Both CT and FLI show the same quantitative trend in which intensity reaches a maximum at 48 h post injection.

Correlating CT Imaging with Live Fluorescence Imaging. A critical step in establishing the proposed cell tracking approach as a reliable and consistent imaging technique is validating that the imaged GNPs are primarily contained within, and not secreted from, the T-cells. Therefore, we compared the CT imaging results with FLI by using the double-labeled T-cells (loaded with GNP for CT imaging and expressing GFP for FLI). We found that the FLI results correlated well with CT results and showed the same trend in signal intensity at the tumor site at all time points (24 h, 48 h, and 5 days post injection). Targeted T-cells demonstrated a distinct increase in the fluorescence signal at the tumor site, peaking at 48 h postcell injection (Figure 10B,C) and decreasing at later time points (up to 5 days post injection) (see Supporting Information, Figure S13). In contrast, nontargeted T-cells demonstrated no increase in signal at the tumor area at any time point

(Figure 10E,F and Supporting Information, Figure S14). This remarkable correlation between imaging modalities indicates that the signal obtained by CT primarily originates from GNPs contained within the targeted T-cells that arrived at the tumor site. Although some percentage of GNPs could have leaked from the T-cells to the tumor environment, we expect the secreted particles to further diffuse and more rapidly to be cleared from the body.

This correlation was further validated by quantitative comparison, over time, between the CT and fluorescence signals at the tumor site in a single mouse treated with targeted T-cells. The results presented in Figure 11 indicate the same quantitative trend in both imaging modalities, showing that the signal intensity reaches a maximum at 48 h. This analysis further validates that the signal obtained by CT is attributable to the presence of the migrated “golden” T-cells.

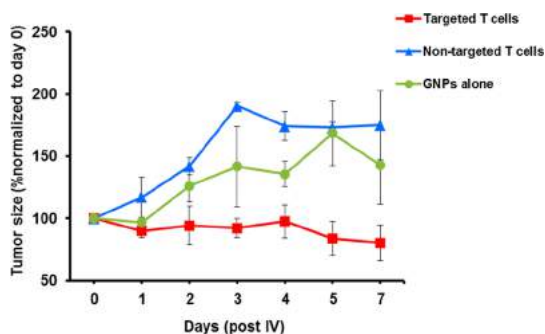


Figure 12. Comparison of tumor growth rate in T-cell-treated mice. Mice were treated with either targeted T-cells labeled with GNPs and GFP, nontargeted T-cells labeled with GNPs and GFP or GNPs only. Results are presented as mean \pm SEM. The difference between targeted and nontargeted groups was statistically significant ($p = 0.0005$).

In Vivo Tumor Regression Mediated by “Golden” T-Cells. To validate the therapeutic effect of the GNP-labeled targeted T-cells *in vivo*, tumor growth was measured with a caliper in a blinded fashion. The calculated results are shown in Figure 12. Following treatment with GNP-labeled targeted T-cells, significant tumor regression was observed compared to control groups treated with GNP-labeled nontargeted T-cells or GNPs alone ($p = 0.0005$). These results confirm that GNPs did not affect antitumor functionality and therapeutic ability of the T-cells.

CONCLUSIONS

This work demonstrates, for the first time, a reliable, real-time, and longitudinal CT imaging technique for tracing immune cells post-transplantation and evaluating their biodistribution, migration, and final fate.

MATERIALS AND METHODS

GNP Synthesis and Conjugation. *Synthesis.* GNPs were prepared using sodium citrate according to the known methodology described by Enustun and Turkevich. First, 0.414 mL of 1.4 M HAuCl_4 solution in 200 mL of water was added to a 250 mL single-neck round-bottom flask and stirred in an oil bath on a hot plate until boiled. Then 4.04 mL of a 10% sodium citrate solution (0.39 M sodium citrate tribasic dihydrate 98%, Sigma CAS 6132-04-3) was then quickly added. The solution was stirred for 5 min, and then the flask was removed from the hot oil and placed aside until cooled.

Conjugation. To prevent aggregation and stabilize the particles in physiological solutions, *O*-(2-carboxyethyl)-*O'*-(2-mercaptoethyl)heptaethylene glycol (PEG7) (95%, Sigma-Aldrich, Israel Ltd.) was absorbed onto the GNPs. This layer also provides the chemical groups required for antibody conjugation ($-\text{COOH}$). First, the solution was centrifuged to dispose of excess citrate. PEG7 solution was then added to the GNP solution, stirred overnight, and put in a centrifuge in order to dispose of excess PEG.

To increase cell-uptake rate, stabilized GNPs were further coated with glucose. Excess *N*-ethyl-*N*-(3-(dimethylamino)propyl) carbodiimide (EDC) and *N*-hydroxysuccinimide (NHS) (Thermo Fisher Scientific, Inc., Rockford, IL) were added to the solution, followed by addition of glucose-2 (2GF) ($\text{D-}(+)\text{-glucosamine hydrochloride}$, Sigma-Aldrich, Israel Ltd.). NHS and EDC form an active ester intermediate with the $-\text{COOH}$

CT imaging, which is commonly applied clinically, not only enabled visualization of the transplanted “golden” T-cells but also provided detailed anatomical information and assisted in elucidating the pathology of the disease. The ability to conduct online tracking of engineered T-cells may assist in elucidating the underlying causes for off-target toxicity and more accurately identify the targeted organs subject to adverse immune reactions in adoptive T-cell transfer-based treatments. Indeed, this is of paramount importance in treatment modalities in which little is known about the antigen distribution, and if coupled with a suicide-gene strategy in a dose-escalation protocol, this could help preventing a possible fatal outcome following gene-modified immune cell administration to patients.

The direct correlation observed between fluorescence imaging and CT imaging of the dual-labeled T-cells demonstrated the reliability of our GNP-based CT imaging method for cell tracking. Moreover, the study revealed that labeling with GNPs did not affect T-cell function, as demonstrated both *in vitro*, by cytokine release and proliferation assays, and *in vivo*, by tumor regression analysis. The results presented in this study have significant research and clinical implications and offer a valuable tool for elucidating poorly understood mechanisms underlying the success or failure of T-cell therapy. Our novel cell tracking approach, which utilizes highly stable and versatile nanoparticles, can advance both adoptive cell transfer-based cancer immunotherapy and other cell-based therapy approaches and could become part of next-generation imaging techniques.

functional groups, which can then undergo an amidation reaction with the glucose $-\text{NH}_2$ group. Glucosamine molecule C-2 (2GF-GNP): $\text{D-}(+)\text{-glucosamine hydrochloride}$ (3 mg; Sigma-Aldrich) was added to the activated linker-coated GNPs.

T-Cell Isolation and Preparation. *Patient PBMCs and Cell Lines.* All of the PBMCs used in this study were from normal donors obtained from the Israeli Blood Bank (Sheba Medical Center, Tel-Hashomer, Israel). Melanoma cell line HLA-A2 $^-$ /MART-1+ 888 was isolated from surgically resected metastases as previously described.⁴⁵ The 888/A2 is a HLA-A2-transduced line derived from the 888 cell line. SK-MEL-23 is a HLA-A2+ melanoma cell line.⁴⁶ Viral packaging line 293GP, which stably expresses GAG and POL proteins, has been previously described.⁴⁷ All cell lines were cultured in DMEM (Invitrogen, Carlsbad, CA), supplemented with 10% heat-inactivated fetal bovine serum (Biological Industries, Beth Haemek, Israel) and were maintained in a 37 °C and 5% CO_2 incubator. Primary human T-Lymphocytes were cultured in BioTarget medium (Biological Industries, Beth Haemek, Israel) supplemented with 10% heat-inactivated FBS and 300 IU/mL IL-2 and maintained at 37 °C and 5% CO_2 .

Retroviral Construct. The α - and β -chains from the previously characterized TCRs specific for MART-126-35 termed F4 (or DMF4)^{31,32} were subcloned into the pMSGV1 vector, as described previously.³¹

Transduction of T-Cells. For virus production, transfection of 2×10^6 293GP cells with 9 μg of DNA of MSGV1-F4 retroviral construct and 4.5 μg of envelope plasmid (VSV-G) was performed

using JetPrime transfection reagent (Polyplus, France). After 4 h, the medium was replaced. Retroviral supernatant was collected 36 h after the DNA transfection. Freshly isolated lymphocytes were stimulated for 48 h in the presence of 50 ng/mL OKT3 (eBioscience, San Diego, CA) before transduction. Following stimulation, lymphocytes were transduced with retroviral vectors by transfer to nontreated tissue culture dishes (Nunc, Rochester NY) that had been precoated with RetroNectin (Takara, Japan) and retroviral vectors as previously described.⁴⁸

Cytokine Release Assay. T-cell cultures were tested for reactivity in cytokine release assay using commercially available ELISA kit for IFN γ (R&D Systems, Minneapolis, MN). For this assay, 1×10^5 responder cells (PBL) and 1×10^5 stimulator cells (tumor cells) were incubated in a 0.2 mL culture volume in individual wells of 96-well plates. Stimulator cells and responder cells were cocultured for 18 h. Cytokine secretion was measured in culture supernatants diluted to be in the linear range of the assay. As a control for T cell activity, we incubated the different T-cell cultures with PHA.

Flow Cytometry Analysis of Cell Proliferation and Viability. Immunofluorescence, analyzed as the relative log fluorescence of live cells, was measured using a CyAn-ADP flow cytometer (Beckman Coulter, Brea). Approximately 1×10^5 cells were analyzed. For cell proliferation assay, T-cells were labeled with 1 μ M CFSE (eBioscience, San Diego, CA) for 6 min and then cultured in the presence of 0.1 mg/mL plate-bound OKT3 (eBioscience, San Diego, CA). Cells fluorescence was analyzed by flow cytometry. Cell viability assays were performed as follows: After T-cell labeling with GNPs, cells were labeled with 1 μ M propidium iodide (PI) (Sigma-Aldrich, Israel) to assess the ratio of cell death. Samples were analyzed by flow cytometry. For the different analysis procedures, cells were incubated in buffer made of PBS, 0.5% BSA, and 0.02% sodium azide.

Statistical Analysis. The results of cytokine secretion were compared using a paired two-tailed Student's *t* test. *p*-Values below 0.05 were considered significant.

Labeling T-Cells with GNPs and Flame. FAAS, SpectraAA140, Agilent Technologies. Labeled T-cells were melted with *aqua regia* acid, a mixture of nitric acid and hydrochloric acid in a volume ratio of 1:3. The samples were then filtered and diluted to a final volume of 5 mL. A Au lamp was used in order to determine the gold concentration in the samples. A calibration curve with known gold concentrations was prepared (commonly: 0.1, 1, 2, and 5 mg/mL). Gold concentration in each sample was determined according to its absorbance value with correlation to the calibration curve. Each sample was analyzed in triplicate, and averages and standard deviations were taken.

Dark-Field Microscopy. A Nikon i50 microscope (Tokyo, Japan) equipped with a hyperspectral imaging system (CRI, USA) was used to obtain dark-field images (20 \times magnification) in order to assess nanoparticle uptake.

Animal Model and Injections. Athymic nude mice were inoculated with SKMEL23 and transduced-GNPs loaded lymphocytes. More specifically, six-week-old athymic nude-Foxn1nu female mice (Harlan, Jerusalem, Israel) were subcutaneously injected with 4×10^6 SKMEL23 cells. After tumor establishment (10–16 days), $16\text{--}20 \times 10^6$ F4-transduced and GNPs loaded lymphocytes were intravenously injected into the mice.

Live Fluorescent Imaging. Fluorescence was studied by the Maestro II in vivo imaging system, 2D planar fluorescence imaging of small animals (Cambridge Research and Instrumentation, Inc., Woburn, MA). A blue excitation/emission filter set was used for our experiments (λ_{ex} , 434–480 nm; λ_{em} > 457 nm). The Liquid Crystal Tunable Filter (LCTF) was programmed to acquire image cubes from $\lambda = 500\text{--}600$ nm with an increment of 10 nm per image. Fluorescence intensity measurements were calculated as average intensity over the tumor surface area by using ImageJ software.

In Vivo Micro-CT Scans. *In vivo* scans of mice were performed with nominal resolution (pixel size) of 36 μ m, employing an aluminum filter 0.2 mm thick and an applied X-ray tube voltage of 45 kV. Surface-rendered 3D models were constructed for 3D viewing of the analyzed mice. Volume rendered 3D images were generated using an RGBA transfer function in SkyScan CT-Volume ("CTVol") software (Skyscan 1176, Bruker micro-CT, Kontich, Belgium), (NRecon v.1.6.9, Bruker micro-CT).

Tumor Growth Measurements. Tumor growth was measured in a blinded fashion using a caliper and calculated using the following formula: $[D \times d^2] \times \Pi/6$, where *D* is the largest tumor diameter and *d* its perpendicular one. In addition, tumor growth was measured by a 3D analysis by CT analyzer software. All of the procedures were performed according to the guidelines of the university committee for animal welfare.

Conflict of Interest: The authors declare no competing financial interest.

Supporting Information Available: CT images of targeted T-cells; CT images of non-targeted T-cells; FLI of targeted T-cells; FLI of on-targeted T-cells. The Supporting Information is available free of charge on the ACS Publications website at DOI: 10.1021/acsnano.5b01939.

Acknowledgment. This work was partially supported by the Israel Cancer Research Fund (ICRF), by the Israel Science Foundation (749/14 and 1457/12), by the Christians for Israel Chair in Medical Research, and by the Shulamit Aloni Scholarship for promotion of women in exact sciences and engineering.

REFERENCES AND NOTES

- Ahrens, E. T.; Bulte, J. W. M. Tracking Immune Cells in Vivo Using Magnetic Resonance Imaging. *Nature Rev. Immunol.* **2013**, *13*, 755–763.
- Janowski, M.; Bulte, J. W. M.; Walczak, P. Personalized Nanomedicine Advancements for Stem Cell Tracking. *Adv. Drug Delivery Rev.* **2012**, *64*, 1488–1507.
- Lindvall, O.; Björklund, A. Cell Therapy in Parkinson's Disease. *NeuroRx* **2004**, *1*, 382–393.
- Bongso, A.; Fong, C.-Y.; Gauthaman, K. Taking Stem Cells to the Clinic: Major Challenges. *J. Cell. Biochem.* **2008**, *105*, 1352–1360.
- Tong, L.; Zhao, H.; He, Z.; Li, Z. Current Perspectives on Molecular Imaging for Tracking Stem Cell Therapy. In *Medical Imaging in Clinical Practice*; ERondu, O. F., Ed. Intech: Rijeka, Croatia, 2013; Chapter 4.
- Srivastava, A. K.; Bulte, J. W. M. Seeing Stem Cells at Work in Vivo. *Stem Cell Rev.* **2014**, *10*, 127–144.
- Jha, P.; Golovko, D.; Bains, S.; Hostetter, D.; Meier, R.; Wendland, M. F.; Daldrup-link, H. E. Monitoring of NK-Cell Immunotherapy Using Non-Invasive Imaging Modalities. *Cancer Res.* **2011**, *70*, 6109–6113.
- Shilo, M.; Reuveni, T.; Motiei, M.; Popovtzer, R. Nanoparticles as Computed Tomography Contrast Agents: Current Status and Future Perspectives. *Nanomedicine (London)* **2012**, *7*, 257–269.
- Yu, S. B.; Watson, A. D. Metal-Based X-Ray Contrast Media. *Chem. Rev.* **1999**, *99*, 2353–2378.
- Khan, M. S.; Vishakante, G. D.; Siddaramaiah, H. Gold Nanoparticles: A Paradigm Shift in Biomedical Applications. *Adv. Colloid Interface Sci.* **2013**, *199–200*, 44–58.
- Nam, S. Y.; Ricles, L. M.; Sokolov, K.; Suggs, L. J.; Emelianov, S. Y. Ultrasound and Photoacoustic Imaging to Monitor Mesenchymal Stem Cells Labeled with Gold Nanoparticles. *Proc. SPIE* **2011**, *Photons Plus Ultrasound: Imaging and Sensing 2011*, 78991Z.
- Chung, E.; Nam, S. Y.; Ricles, L. M.; Emelianov, S. Y.; Suggs, L. J. Evaluation of Gold Nanotracers to Track Adipose-Derived Stem Cells in a PEGylated Fibrin Gel for Dermal Tissue Engineering Applications. *Int. J. Nanomed.* **2013**, *8*, 325–336.
- Nam, S. Y.; Ricles, L. M.; Suggs, L. J.; Emelianov, S. Y. In Vivo Ultrasound and Photoacoustic Monitoring of Mesenchymal Stem Cells Labeled with Gold Nanotracers. *PLoS One* **2012**, *7*, e37267.
- Jokerst, J. V.; Thangaraj, M.; Kempen, P. J.; Sinclair, R.; Sanjiv, S. Photoacoustic Imaging of Mesenchymal Stem Cells in Living Mice via Silica-Coated Gold Nanorods. *ACS Nano* **2013**, *6*, 5920–5930.
- Meir, R.; Motiei, M.; Popovtzer, R. Gold Nanoparticles for in Vivo Cell Tracking. *Nanomedicine (London)* **2014**, *9*, 2059–2069.

16. Menk, R. H.; Schültke, E.; Hall, C.; Arfelli, F.; Astolfo, A.; Rigon, L.; Round, A.; Ataelmannan, K.; MacDonald, S. R.; Juurlink, B. H. J. Gold Nanoparticle Labeling of Cells Is a Sensitive Method to Investigate Cell Distribution and Migration in Animal Models of Human Disease. *Nanomedicine* **2011**, *7*, 647–654.
17. Astolfo, A.; Schültke, E.; Menk, R. H.; Kirch, R. D.; Juurlink, B. H. J.; Hall, C.; Harsan, L.-A.; Stebel, M.; Barbetta, D.; Tromba, G.; Arfelli, F. In Vivo Visualization of Gold-Loaded Cells in Mice Using X-Ray Computed Tomography. *Nanomedicine: Nanotechnol., Biol. Med.* **2013**, *9*, 284–292.
18. Schültke, E.; Menk, R.; Pinzer, B.; Astolfo, A.; Stampanoni, M.; Arfelli, F.; Harsan, L.-A.; Nikkhah, G. Single-Cell Resolution in High-Resolution Synchrotron X-Ray CT Imaging with Gold Nanoparticles. *J. Synchrotron Radiat.* **2014**, *21*, 242–250.
19. Astolfo, A.; Arfelli, F.; Schültke, E.; James, S.; Mancini, L.; Menk, R.-H. A Detailed Study of Gold-Nanoparticle Loaded Cells Using X-Ray Based Techniques for Cell-Tracking Applications with Single-Cell Sensitivity. *Nanoscale* **2013**, *5*, 3337–3345.
20. Shilo, M.; Motiei, M.; Hana, P.; Popovtzer, R. Transport of Nanoparticles through the Blood–Brain Barrier for Imaging and Therapeutic Applications. *Nanoscale* **2014**, *6*, 2146–2152.
21. Wang, Y.; Xu, C.; Ow, H. Commercial Nanoparticles for Stem Cell Labeling and Tracking. *Theranostics* **2013**, *3*, 544–560.
22. Rosenberg, S. A.; Restifo, N. P. Adoptive Cell Transfer as Personalized Immunotherapy for Human Cancer. *Science* **2015**, *348*, 62–68.
23. Chen, Y.-S.; Shen, C.-R. Immune Checkpoint Blockade Therapy: The 2014 Tang Prize in Biopharmaceutical Science. *Biomed. J.* **2015**, *38*, 5–8.
24. Ascierto, P. A. Immunotherapies and Novel Combinations: The Focus of Advances in the Treatment of Melanoma. *Cancer Immunol. Immunother.* **2014**, *64*, 271–274.
25. Weber, J.; Atkins, M.; Hwu, P.; Radvanyi, L.; Sznol, M.; Yee, C. Immunotherapy Task Force of the NCI Investigational Drug Steering Committee. White Paper on Adoptive Cell Therapy for Cancer with Tumor-Infiltrating Lymphocytes: A Report of the CTEP Subcommittee on Adoptive Cell Therapy. *Clin. Cancer Res.* **2011**, *17*, 1664–1673.
26. Rosenberg, S. A.; Dudley, M. E. Adoptive Cell Therapy for the Treatment of Patients with Metastatic Melanoma. *Curr. Opin. Immunol.* **2009**, *21*, 233–240.
27. Johnson, L. A.; Morgan, R. A.; Dudley, M. E.; Cassard, L.; Yang, J. C.; Hughes, M. S.; Kammula, U. S.; Royal, R. E.; Sherry, R. M.; Wunderlich, J. R.; Lee, C.-C. R.; Restifo, N. P.; Schwarz, S. L.; Cogdill, A. P.; Bishop, R. J.; Kim, H.; Brewer, C. C.; Rudy, S. F.; VanWaes, C.; Davis, J. L.; Mathur, A.; Ripley, R. T.; Nathan, D. A.; Laurencot, C. M.; Rosenberg, S. A. Gene Therapy with Human and Mouse T-Cell Receptors Mediates Cancer Regression and Targets Normal Tissues Expressing Cognate Antigen. *Blood* **2009**, *114*, 535–546.
28. Restifo, N. P.; Dudley, M. E.; Rosenberg, S. A. Adoptive Immunotherapy for Cancer: Harnessing the T Cell Response. *Nature Rev. Immunol.* **2012**, *12*, 269–281.
29. Merhavi-Shoham, E.; Haga-Friedman, A.; Cohen, C. J. Genetically Modulating T-Cell Function to Target Cancer. *Semin. Cancer Biol.* **2012**, *22*, 14–22.
30. Daniel-Meshulam, I.; Ya'acobi, S.; Ankri, C.; Cohen, C. J. How (specific) Would like Your T-Cells Today? Generating T-Cell Therapeutic Function through TCR-Gene Transfer. *Front. Immunol.* **2012**, *3*, 186.
31. Morgan, R. A.; Dudley, M. E.; Wunderlich, J. R.; Hughes, M. S.; Yang, J. C.; Sherry, R. M.; Royal, R. E.; Topalian, S. L.; Kammula, U. S.; Restifo, N. P.; Zheng, Z.; Nahvi, A.; de Vries, C. R.; Rogers-Freezer, L. J.; Mavroukakis, S. A.; Rosenberg, S. A. Cancer Regression in Patients after Transfer of Genetically Engineered Lymphocytes. *Science* **2006**, *314*, 126–129.
32. Cohen, C. J.; Zhao, Y.; Zheng, Z.; Rosenberg, S. A.; Morgan, R. A. Enhanced Antitumor Activity of Murine–Human Hybrid T-Cell Receptor (TCR) in Human Lymphocytes Is Associated with Improved Pairing and TCR/CD3 Stability. *Cancer Res.* **2006**, *66*, 8878–8886.
33. Cohen, C. J.; Li, Y. F.; El-Gamil, M.; Robbins, P. F.; Rosenberg, S. A.; Morgan, R. A. Enhanced Antitumor Activity of T Cells Engineered to Express T-Cell Receptors with a Second Disulfide Bond. *Cancer Res.* **2007**, *67*, 3898–3903.
34. Bialer, G.; Horovitz-Fried, M.; Ya'acobi, S.; Morgan, R. A.; Cohen, C. J. Selected Murine Residues Endow Human TCR with Enhanced Tumor Recognition. *J. Immunol.* **2010**, *184*, 6232–6241.
35. Haga-Friedman, A.; Horovitz-Fried, M.; Cohen, C. J. Incorporation of Transmembrane Hydrophobic Mutations in the TCR Enhance Its Surface Expression and T Cell Functional Avidity. *J. Immunol.* **2012**, *188*, 5538–5546.
36. Daniel-Meshulam, I.; Horovitz-Fried, M.; Cohen, C. J. Enhanced Antitumor Activity Mediated by Human 4–1BB-Engineered T Cells. *Int. J. Cancer* **2013**, *133*, 2903–2913.
37. Ankri, C.; Shamalov, K.; Horovitz-Fried, M.; Mauer, S.; Cohen, C. J. Human T Cells Engineered to Express a Programmed Death 1/28 Costimulatory Retargeting Molecule Display Enhanced Antitumor Activity. *J. Immunol.* **2013**, *191*, 4121–4129.
38. Betzer, O.; Shwartz, A.; Motiei, M.; Kazimirsky, G.; Gispán, I.; Damti, E.; Brodie, C.; Yadid, G.; Popovtzer, R. Nanoparticle-Based CT Imaging Technique for Longitudinal and Quantitative Stem Cell Tracking within the Brain: Application in Neuropsychiatric Disorders. *ACS Nano* **2014**, *8*, 9274–9285.
39. Enustun, B. V.; Turkevich, J. Coagulation of Colloidal Gold. *J. Am. Chem. Soc.* **1963**, *85*, 3317–3328.
40. Popovtzer, R.; Agrawal, A.; Kotov, N. A.; Popovtzer, A.; Balter, J.; Carey, T. E.; Kopelman, R. Targeted Gold Nanoparticles Enable Molecular CT Imaging of Cancer. *Nano Lett.* **2008**, *8*, 4593–4596.
41. Hughes, M. S.; Yu, Y. Y. L.; Dudley, M. E.; Zheng, Z.; Robbins, P. F.; Li, Y.; Wunderlich, J.; Hawley, R. G.; Moayeri, M.; Rosenberg, S. A.; Morgan, R. A. Transfer of a TCR Gene Derived from a Patient with a Marked Antitumor Response Conveys Highly Active T-Cell Effector Functions. *Hum. Gene Ther.* **2005**, *16*, 457–472.
42. Gu, E.; Chen, W.-Y.; Gu, J.; Burrridge, P.; Wu, J. C. Molecular Imaging of Stem Cells: Tracking Survival, Biodistribution, Tumorigenicity, and Immunogenicity. *Theranostics* **2012**, *2*, 335–345.
43. Gastman, B. R.; Johnson, D. E.; Whiteside, T. L.; Rabinowich, H. Tumor-Induced Apoptosis of T Lymphocytes: Elucidation of Intracellular Apoptotic Events. *Blood* **2000**, *95*, 2015–2023.
44. Meyerrose, T. E.; Herrbrich, P.; Hess, D. A.; Nolte, J. A. Immune-Deficient Mouse Models for Analysis of Human Stem Cells. *Biotechniques* **2003**, *35*, 1262–1272.
45. Topalian, S. L.; Solomon, D.; Rosenberg, S. A. Tumor-Specific Cytotoxicity by Lymphocytes Infiltrating Human Melanomas. *J. Immunol.* **1989**, *142*, 3714–3725.
46. Houghton, A. N.; Real, F. X.; Davis, L. J.; Cordon-Cardo, C.; Old, L. J. Phenotypic Heterogeneity of Melanoma. Relation to the Differentiation Program of Melanoma Cells. *J. Exp. Med.* **1987**, *165*, 812–829.
47. Wargo, J. A.; Robbins, P. F.; Li, Y.; Zhao, Y.; El-Gamil, M.; Caragacianu, D.; Zheng, Z.; Hong, J. A.; Downey, S.; Schrumpp, D. S.; Rosenberg, S. A.; Morgan, R. A. Recognition of NY-ESO-1⁺ Tumor Cells by Engineered Lymphocytes Is Enhanced by Improved Vector Design and Epigenetic Modulation of Tumor Antigen Expression. *Cancer Immunol. Immunother.* **2009**, *58*, 383–394.
48. Goff, S. L.; Johnson, L. A.; Black, M. A.; Xu, H.; Zheng, Z.; Cohen, C. J.; Morgan, R. A.; Rosenberg, S. A.; Feldman, S. A. Enhanced Receptor Expression and in Vitro Effector Function of a Murine–Human Hybrid MART-1-Reactive T Cell Receptor Following a Rapid Expansion. *Cancer Immunol. Immunother.* **2010**, *59*, 1551–1560.